Comparing the Extended and the Sigma Point Kalman Filters for Orbit Determination Modeling Using GPS Measurements

3 authors:

Paula Cristiane Pinto Mesquita Pardal
University of São Paulo
29 PUBLICATIONS   **118** CITATIONS

SEE PROFILE

Helio Koiti Kuga
National Institute for Space Research, Brazil
264 PUBLICATIONS   **803** CITATIONS

SEE PROFILE

Rodolpho Vilhena de Moraes
São Paulo State University
142 PUBLICATIONS   **635** CITATIONS

SEE PROFILE

Some of the authors of this publication are also working on these related projects:

Project   My dissertation of M.Sc. View project

Project   CONASAT View project

Comparing the Extended and the Sigma Point Kalman Filters for Orbit Determination Modeling Using GPS Measurements

P.C.P.M. Pardal, H.K. Kuga, INPE (*Brazilian Space Research Institute*)
R. Vilhena de Moraes, FEG - UNESP (*The State of São Paulo University*)

BIOGRAPHIES

Pardal is PhD. student in aerospace engineering and technology, with emphasis in space mechanics and control, at Brazilian Space Research Institute (INPE). She is presently focusing on algorithms of orbit determination via GPS. Her e-mail is paulacristiane@gmail.com
Kuga is Dr. in Space Engineering and Technology (1989) at Brazilian Space Research Institute (INPE). Senior engineer at INPE. Current researches include orbital dynamics, stability and control of artificial satellites, mission analysis, orbit and attitude determination, GPS data processing, and Kalman filtering applications. His e-mail is hkk@dem.inpe.br
Vilhena de Moraes is Dr. in Orbital Mechanics and Flight Dynamics at Aeronautical Institute of Technology (ITA), Brazil. Full Professor from 1963 to 1995 at ITA. Since 1995, Assistant Doctor Professor at the Department of Mathematics at UNESP/FEG, campus of Guaratinguetá, SP, Brazil. His current researches include celestial Mechanics, astrodynamics, and orbit determination. His e-mail is rodolpho@feg.unesp.br

ABSTRACT

The purpose of this work is to compare the extended Kalman filter (EKF) against the nonlinear sigma point Kalman filter (SPKF) for the satellite orbit determination problem, using GPS measurements. The comparison is based on the levels of accuracy improvement of the orbit dynamics model. The main subjects for the comparison between the estimators are accuracy of models and results. Based on the analysis of such criteria, the advantages and drawbacks of each estimator are presented.
In this work, the orbit of an artificial satellite is determined using real data from the Global Positioning System (GPS) receivers. In orbit determination of artificial satellites, the dynamic system and the measurements equations are of nonlinear nature. It is a nonlinear problem in which the disturbing forces are not easily modeled. The problem of orbit determination consists essentially of estimating parameter values that

completely specify the body trajectory in the space, processing a set of information (measurements) related to this body. Such observations can be collected through a ground tracking network on Earth or through sensors, like space GPS receivers onboard the satellite.
The EKF implementation in orbit estimation, under inaccurate initial conditions and scattered measurements, can lead to unstable or diverging solutions. For solving the problem of nonlinear nature, convenient extensions of the Kalman filter have been sought. In particular, the unscented transformation was developed as a method to propagate mean and covariance information through nonlinear transformations. The Sigma Point Kalman Filter (SPKF) appears as an emerging estimation algorithm applied to nonlinear systems, without needing linearization steps.
In this orbit determination case study the focus is to gradually improve the dynamical model, which presents highly nonlinear properties, and to know how it affects the performance of the estimators. Therefore, the EKF (the most widely used real time estimation algorithm) as well as the SPKF (supposedly one of the most appropriate estimation algorithm for nonlinear systems) performance evaluation is justified.
The aim of this work is to analyze the new nonlinear estimation technique, the SPKF, in an actual orbit determination problem with actual measurements data from GPS, and to compare it with a widely used technique, the EKF, pinpointing the main differences between both the algorithms.

INTRODUCTION

In orbit determination of artificial satellites, both the dynamic system and the measurements equations are of nonlinear nature. It is a nonlinear problem in which the disturbing forces are not easily modeled. The problem consists of estimating variables that completely specify the body trajectory in the space, processing a set of information (pseudo-range measurements) related to this body. The more accurate GPS phase measurements are not used here, because the aim is not the search for accuracy, but a comparison of performance under different levels of orbit models. Besides with carrier

phase measurements, the ambiguity resolution algorithm could eventually mask the results.

A space borne GPS receiver is a powerful means to determine orbits of artificial Earth satellites by providing many redundant measurements. The Topex/Poseidon (T/P) is an example of using GPS for space positioning. Through an onboard GPS receiver, the pseudo-ranges (pseudo-distance from satellite to each of the tracked GPS satellites) related to the body can be measured and can be used to estimate the orbital state.

The EKF is probably the most widely used real time estimation algorithm for nonlinear systems. The EKF is a nonlinear version of the Kalman filter (KF) that generates reference trajectories which are updated at the time of each measurement processing. However, the experience from the estimation community has shown that it is difficult to implement, requires some skill to tune, and is only reliable for systems that are nearly linear on the time scale of the filter working updates. Many of these difficulties arise from the linearized approximations needed by the EKF method. Specifically for the orbit estimation problem, under inaccurate initial conditions and scattered measurements, the EKF implementation can lead to unstable or diverging solutions. Therefore, there is a strong need for a method that is more accurate than linearization, but at the same time does not increase neither the implementation nor additional computational costs like other higher order filtering schemes. To overcome this limitation, the unscented transformation was developed as a technique to propagate mean and covariance information through nonlinear transformations. The SPKF is a new estimator that claims to yield equivalent or better performance than the EKF and elegantly is applied to nonlinear systems, without the linearization steps. This algorithm is a new approach to generalize the KF for nonlinear process and observation models.

THE EXTENDED KALMAN FILTER

The EKF is a nonlinear version of the KF that generates reference trajectories which are updated at each measurement processing times (Brown and Hwang, 1985).

Due to the complexity of accurately modeling the nonlinear satellite orbit, the EKF is generally used in works of such nature. The algorithm always provides up to date reference trajectory around the most current available estimate.

Exploiting the assumption that all transformations are quasi-linear, the EKF simply linearizes all nonlinear transformations and substitutes the Jacobian matrices for the linear transformations in the KF equations. The EKF consists of cycles of time and measurement updates. In the first, state and covariance are propagated from one previous instant to a later one, meaning that they are propagated between discrete instants of the system dynamics model. In the second one, state and covariance are corrected for the later instant corresponding to the measurement time, through the observations model. This method has recursive nature and does not need to store the measurements previously in large matrices, being therefore well suited for real time processing.

The EKF time update cycle is given by

$$\dot{\bar{\mathbf{x}}}_k = \mathbf{f}(\hat{\mathbf{x}}_{k-1})$$
$$\bar{\mathbf{P}}_k = \boldsymbol{\varphi}_{k,k-1}\hat{\mathbf{P}}_{k-1}\boldsymbol{\varphi}_{k,k-1}^T + \mathbf{Q}_k$$

where $\mathbf{f}$ is a nonlinear vector function modeling the orbit motion, $\bar{\mathbf{x}}_k$ and $\bar{\mathbf{P}}_k$ are respectively the propagated state and the covariance for t_k; φ is the state transition matrix between t_{k-1} e t_k; $\mathbf{Q}_k$ is the dynamics noise matrix given by

$$\mathbf{Q}_k = \int_{t_{k-1}}^{t_k} \boldsymbol{\varphi}(t, t_{k-1})\mathbf{G(t)}\mathbf{Q(t)}\mathbf{G}^T(t)\boldsymbol{\varphi}^T(t, t_{k-1})dt$$

The equations for the EKF measurement update cycle are

$$\mathbf{K}_k = \bar{\mathbf{P}}_k\mathbf{H}_k^T(\mathbf{H}_k\bar{\mathbf{P}}_k\mathbf{H}_k^T + \mathbf{R}_k)^{-1}$$
$$\hat{\mathbf{P}}_k = (\mathbf{I} - \mathbf{K}_k\mathbf{H}_k)\bar{\mathbf{P}}_k$$
$$\hat{\mathbf{x}}_k = \bar{\mathbf{x}}_k + \mathbf{K}_k\left[\mathbf{y}_k - \mathbf{h}_k\left(\bar{\mathbf{x}}_k\right)\right]$$

where $\mathbf{h}_k$ is a nonlinear vector function modeling the measurements; $\mathbf{H}$ is the Jacobian matrix $\left(\dfrac{\partial \mathbf{h}}{\partial \mathbf{x}}\right)$; $\mathbf{K}_k$ is the Kalman gain; $\hat{\mathbf{x}}$ and $\hat{\mathbf{P}}$ are the state vector and the covariance updated for the instant k.

There are some limitations for the EKF. For example: linearized transformations are reliable only if the error propagation can be matched with good approximation by a linear function; linearization can be applied only if the Jacobian matrix exists; and obtaining the analytical Jacobian matrices can be a very difficult and error-prone process. Summarizing, linearization, as applied in the EKF, is widely recognized to be inadequate, but other alternatives yield substantial costs in terms of derivation and computational complexity. The sigma point algorithms via unscented transformation were developed in an attempt to meet these needs.

THE SIGMA POINT KALMAN FILTER

If the system dynamics and the observation model are linear, the conventional KF can be used fearlessly. However because, not rarely, the system dynamics and/or the measurement models are nonlinear, convenient extensions of the KF like EKF have been used.

The SPKF is a new estimator that allows similar performance than the KF for linear systems and elegantly extends to nonlinear systems, without the linearization steps. This algorithm family is a new approach to generalize the KF for nonlinear process and observation models. A set of weighted samples, the sigma points, is

2733

used for computing mean and covariance of a probability distribution. Such algorithms include the unscented Kalman filter (UKF), which is based on the unscented transformation (UT), a nonlinear transformation for mean and covariance.

The SPKF is a technique claimed to lead to a more accurate and easier to implement filter than the EKF or a second order Gaussian filter. The SPKF approach is described, as follows (van der Merwe et al., 2004)

1. A set of weighted samples is deterministically calculated, based on mean and covariance decomposition of a random variable.
2. The sigma points are propagated through the real nonlinear function, using only functional estimation, that is, analytical derivatives are not used to generate *a posteriori* set of sigma points.
3. The later statistics are calculated using propagated sigma points functions and weights. In general, they assume the form of a simple weighted average of the mean and the covariance.

Herein, it will be described the UT and the UKF, the filter steamming from this transformation.

THE UNSCENTED TRANSFORMATION

The UT is a method to calculate the statistics of a random variable that passes through a nonlinear transformation. The UT approach chooses a set of points (sigma points) so that their mean and covariance are $\overline{\mathbf{x}}$ and $\mathbf{P}_{xx}$ (Julier and Uhlmann, 1997, 2004). The nonlinear function is applied to each point, in turn, to yield a cloud of transformed points. The statistics of the transformed points (mean $\overline{\mathbf{y}}$ and covariance $\mathbf{P}_{yy}$ predicted) can then be calculated to form an estimate of the non linearly transformed mean and covariance.

The sigma points are deterministically chosen so that they exhibit certain specific properties (given mean and covariance, for example), and are not drawn at random. Besides, they can be weighted in ways that are inconsistent with the distribution interpretation of sample points like in a particle filter.

The *n*-dimensional random variable $\mathbf{x}$ with $\overline{\mathbf{x}}$ mean and $\mathbf{P}_{xx}$ covariance is approximated by $2n + 1$ weighted points, given by

$$\boldsymbol{\chi}_0 = \overline{\mathbf{x}}$$
$$\boldsymbol{\chi}_i = \overline{\mathbf{x}} + \left(\sqrt{(n+\kappa)\mathbf{P}_{\mathbf{xx}}} \right)_i$$
$$\boldsymbol{\chi}_{i+n} = \overline{\mathbf{x}} - \left(\sqrt{(n+\kappa)\mathbf{P}_{\mathbf{xx}}} \right)_i$$

in which $\kappa \in \Re$, $\left(\sqrt{(n+\kappa)\mathbf{P}_{\mathbf{xx}}} \right)_i$ is the i-th row or column of the square root matrix of $(n+\kappa)\mathbf{P}_{\mathbf{xx}}$. W_i is the weight associated to the i-th point by

$$W_0 = \frac{\kappa}{(n+\kappa)}$$
$$W_i = \frac{1}{2(n+\kappa)}, \ i = 1,\ldots,n$$
$$W_{i+n} = \frac{1}{2(n+\kappa)}, \ i = 1,\ldots,n$$

The transformation occurs as follows

1. Transform each point through the nonlinear function to yield the set of transformed sigma points

$$y_i = \mathbf{f}[\boldsymbol{\chi}_i]$$

2. The observations mean is given by the weighted average of the transformed points

$$\overline{\mathbf{y}} = \sum_{i=0}^{2n} W_i \, y_i$$

3. The covariance is the weighted outer product of the transformed points

$$\mathbf{P}_{yy} = \sum_{i=0}^{2n} W_i \left[y_i - \overline{\mathbf{y}} \right] \left[y_i - \overline{\mathbf{y}} \right]^{\mathrm{T}}$$

Despite its apparent simplicity, the UT has a number of important properties

1. It works as a "black box" filtering library: given a model, a standard routine can be used to calculate the predicted quantities as necessary for any given transformation.
2. The computational cost of the algorithm may be almost the same order of magnitude as the EKF.
3. Any set of sigma points that encodes the mean and covariance correctly calculates the projected mean and covariance correctly to the second order at least.
4. The algorithm can be used with discontinuous transformations. Sigma points can pass over a discontinuity and, thus, can approximate the effect of a discontinuity on the transformed estimate.

THE UNSCENTED KALMAN FILTER

Using UT, the following steps are processed in the KF

1. Predict the new state system $\hat{\mathbf{x}}(k+1 \,|\, k)$ and its associated covariance $\mathbf{P}(k+1 \,|\, k)$, taking into account the effects of the gaussian white noise process.

2. Predict the expected observation $\hat{\mathbf{y}}(k+1|k)$ and its residual innovation matrix $\mathbf{P}_{vv}(k+1|k)$ considering the effects of the observation noise.
3. Predict the cross correlation matrix $\mathbf{P}_{xy}(k+1|k)$.

Fig. 1 shows these 3 steps of the UT, changing the EKF, in order to lead to the new filter: the UKF. These steps are put in order in the EKF with the re-structuring of dynamics, state vector and observations models.
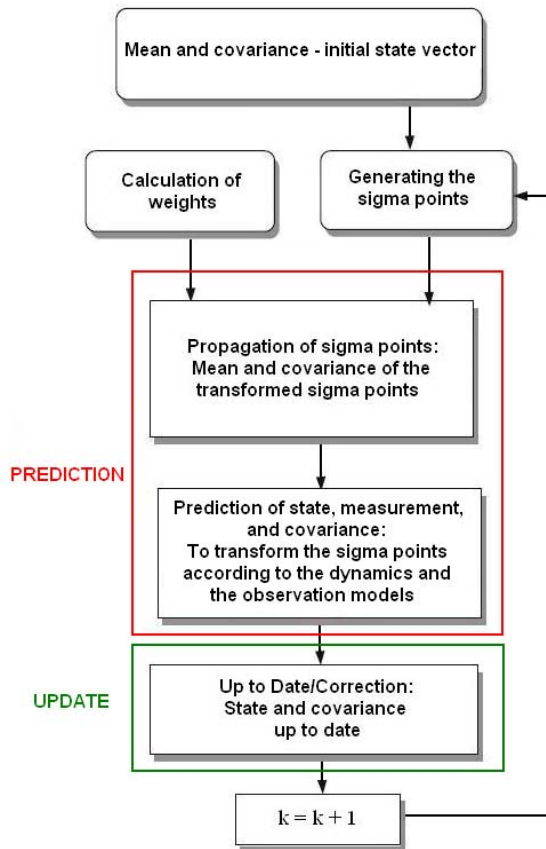

Figure 1. UT introduced in the EKF, leading to UKF

THE ORBIT DETERMINATION

The instantaneous orbit determination using GPS satellites is basically a geometric method. In this method, the observer knows the set of satellites position in the reference system, obtaining its own position in the same reference frame. Fig. 2 presents the basic parameters used by GPS for user position determination. In Fig. 2, $\vec{R}_{GPSi}$ is the position of i-th GPS satellite in the reference system; $\vec{\rho}_i$ is the pseudorange; and $\vec{r}_u$ is the user satellite position in the reference system.
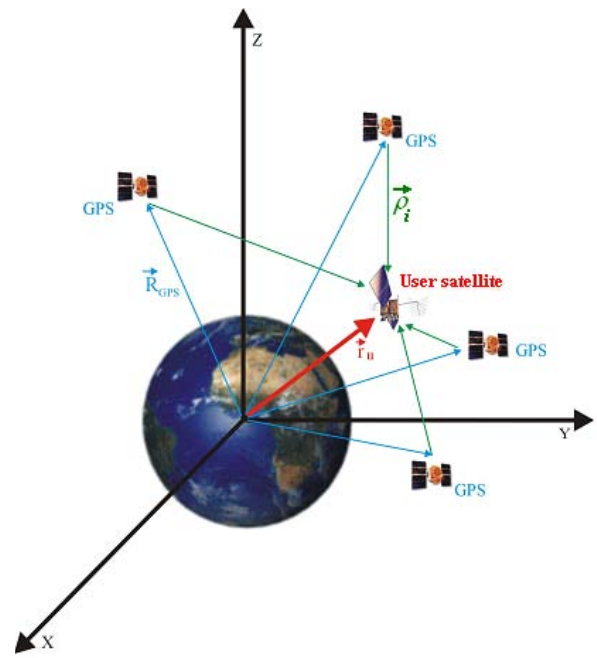

Figure 2. The Geometric Method

However sequential orbit determination makes use of the orbit dynamical model to predict between measurement times and measurement model to update the orbit by processing of GPS measurements. This gives rise to using recursive and real time KF estimator to the orbit determination (Chiaradia et al., 2003).

THE DYNAMIC MODEL

In the case of orbit determination via GPS, the ordinary differential equations that represent the dynamic model are in its simplest form give traditionally as follows

$$\dot{\vec{r}} = \vec{v}$$
$$\dot{\vec{v}} = -\mu\frac{\vec{r}}{r^3} + \vec{a} + \vec{w}$$
$$\dot{b} = d$$
$$\dot{d} = 0 + w_d$$

with variables given in the inertial reference frame. In the equations above, $\vec{r}$ is a vector of the position components vector (x, y, z); $\vec{v}$ is velocity vector; $\vec{a}$ represents the modeled perturbations vector; $\vec{w}$ is the white noise vector with covariance Q; b is the user clock bias; d is the user clock drift; and w_d is the white noise on the drift rate with variance Q_d.

2735

THE FORCE MODEL - PERTURBATIONS CONSIDERED IN THE MODELING

The main disturbing forces of gravitational nature that affect the orbit of an Earth's artificial satellite are: the non uniform distribution of Earth's mass; ocean and terrestrial tides; and the gravitational attraction of the Sun and the Moon. There are also the non gravitational effects, such as: Earth atmospheric drag; direct and reflected solar radiation pressure; electric drag; emissivity effects; relativistic effects; and meteorites impacts.

The disturbing effects are in general included according to the physical situation presented and to the accuracy that is intended for the orbit determination. Here we include only the minimum perturbations set to allow us to assess the performance of both filters.

Geopotential

The Earth is not a perfect sphere with homogeneous mass distribution, and cannot be considered as a material point. Such irregularities disturb the orbit of an artificial satellite and the keplerian elements that describe the orbit do not behave ideally. The potential function can be given by (Kaula, 1966):

$$U(r,\phi,\lambda) = \frac{\mu}{r} \sum_{n=0}^{\infty} \sum_{m=0}^{n} \left(\frac{R_{\mathrm{T}}}{r}\right)^n P_{nm}(\sin\phi) \times$$
$$\times (C_{nm}\cos m\lambda + S_{nm}\sin m\lambda)$$

where μ is Earth gravitational constant; R_{T} is mean Earth radius; r is the spacecraft radial distance; ϕ is the geocentric latitude; λ is the longitude on Earth fixed coordinates system; C_{nm} and S_{nm} are the normalized harmonic spherical coefficients, of degree n and order m; P_{nm} are the associated Legendre functions. The constants μ, R_{T}, C_{nm}, and S_{nm} determine a particular gravitational potential model.

Direct Solar Radiation Pressure

The solar radiation pressure is a non gravitational force that disturbs the motion of an artificial satellite. The way as the perturbation due to solar radiation pressure will affect the keplerian elements depends on the model adopted (if it includes or not shadow, for example). In the general case, it causes secular and periodic perturbations on the Keplerian variables (ω, Ω, M) and also to a less extent on the metric variables (a, e, i).

The components of solar radiation pressure force can be expressed in several systems. Throughout these systems, the orbital elements of the satellite can be connected with Sun's position. This procedure was used here, for the direct solar radiation pressure model adopted for the TOPEX/Poseidon (T/P) satellite (Marshall et al., 1991). Since the force due to the emerging radiation flux on the surface of the satellite depends on the angle of incidence, the attitude of the satellite must be also taken into account.

As Topex/Poseidon (T/P) satellite real data are used to validate the estimation results in this work, the total direct solar radiation pressure acting on T/P, according to Marshall and Luthcke's model (Marshall and Luthcke, 1994) is:

$$\vec{F}_k = \frac{GA_k\cos\theta_k}{c}\left[2\left(\frac{\delta_k}{3} + \rho\cos\theta_k\right)\hat{n}_k + (1-\rho_k)\hat{s}\right]$$
$$\Rightarrow \quad \vec{F} = \sum_{k=1}^{8}\vec{F}_k$$

where G is solar radiant flux (W/m^2); A is the surface area of each plate (m^2); δ is diffusive reflectivity, percentage of the total incoming radiation; ρ is specular reflectivity, percentage of the total incoming radiation; $\hat{n}$ is surface normal vector; $\hat{s}$ is source incidence vector; θ is the angle between surface normal and solar incidence; and c is the speed of light (m/s). Subscript k varies from 1 to 8, representing each satellite plate, and $\vec{F}$ is the total direct solar radiation force acting on the satellite.

Sun-Moon Gravitational Attraction

These perturbations are due to Sun and Moon attraction force and they can be meaningful if the satellite is far from Earth. As the orbital variations are of the same type, be the Sun or the Moon the attractive body, they should be studied without distinguishing the third body. The luni-solar gravitational attraction mainly acts on Ω and ω, what causes precession of the orbit and the orbital plane.

The general three-body problem model is here simplified by the circular restricted three-body problem, where the orbital motion of a third body, which mass can be neglected, around two other massive bodies is studied. The motion equation that provides the third body acceleration can be expressed as (Prado and Kuga, 2001)

$$\ddot{\vec{r}}_3 = -Gm_1\frac{\vec{r}_{13}}{r_{13}^3} - Gm_2\frac{\vec{r}_{23}}{r_{23}^3}$$

where $\vec{r}_{13} = \vec{r}_3 - \vec{r}_1$, $\vec{r}_{23} = \vec{r}_3 - \vec{r}_2$, and $\vec{r}_i$, $i=1,2,3$ is the i-th body distance to the system center of mass.

THE OBSERVATIONS MODEL

The nonlinear equation of the observations model is

$$\mathbf{y}_k = \mathbf{h}_k(\mathbf{x}_k, t) + \mathbf{v}_k$$

where, at time t_k, $\mathbf{y}_k$ is the vector of m observations; $\mathbf{h}_k(\mathbf{x}_k)$ is the nonlinear function of state $\mathbf{x}_k$, with dimension m; and $\mathbf{v}_k$ is the observation errors vector, with dimension m and covariance $\mathbf{R}_k$.

APPLYING UKF ON ORBIT DETERMINATION

With that application in mind, it is now possible to establish the UKF framework.

Because the noise enters additively in both the force and the observation model, the state dimension is the original $n = 8$ (position, velocity, clock offset, clock drift). In this work application one uses actual GPS pseudo-range measurements which are non linearly modeled as well.

Next, the set of sigma points is built

$$\boldsymbol{\chi}_{0,k} = \overline{\mathbf{x}}_k$$

$$\boldsymbol{\chi}_{i,k} = \overline{\mathbf{x}}_k + \left(\sqrt{(n+\lambda)\mathbf{P}_k} \right)_i, \ i = 1,\dots,n$$

$$\boldsymbol{\chi}_{i,k} = \overline{\mathbf{x}}_k - \left(\sqrt{(n+\lambda)\mathbf{P}_k} \right)_i, \ i = n+1,\dots,2n$$

where $\lambda = \alpha^2(n+\kappa)-n$, with α usually chosen small, in the interval $10^{-4} \le \alpha \le 1$, control the sigma points scatter about the mean $\overline{\mathbf{x}}_k$ (Jwo and Lai, 2008); κ provides an extra degree of freedom; and $\left(\sqrt{(n+\lambda)\mathbf{P}_k} \right)_i$ is the i-th row or column of the root square matrix of $(n+\lambda)\mathbf{P}_k$.

In the propagation step, mean and covariance of the propagated sigma points are used to calculate algebraically the state and the covariance predicted. These sigma points were transformed from the state vector and the dynamical noise.

$$\hat{\mathbf{x}}_{k+1}^- = \sum_{i=0}^{2n} W_i \, \boldsymbol{\chi}_{i,k+1}$$

$$\hat{\mathbf{P}}_{k+1}^- = \sum_{i=0}^{2n} W_i \left[\boldsymbol{\chi}_{i,k+1} - \hat{\mathbf{x}}_{k+1}^- \right]\left[\boldsymbol{\chi}_{i,k+1} - \hat{x}_{k+1}^- \right]^{\mathrm{T}} + \mathbf{Q}_{k+1}$$

The observation vector and the innovation matrix, $\mathbf{P}_{k+1}^{vv}$, are also predicted from mean and covariance of the transformed sigma points on the measurements

$$\begin{cases} y_{0,k+1} = \mathbf{h}_{k+1}\left(\boldsymbol{\chi}_{0,k+1}, t_{k+1} \right) \\ y_{i,k+1} = \mathbf{h}_{k+1}\left(\boldsymbol{\chi}_{i,k+1}, t_{k+1} \right), i = 1,\dots,2n \end{cases}$$

where $\boldsymbol{\chi}$ is built as before. Therefore

$$\hat{\mathbf{y}}_{k+1}^- = \sum_{i=0}^{2n} W_i^{(\mathrm{m})} \, y_{i,k+1}.$$

In this equation, $y_{i,k+1}$ represents the sigma vectors propagated through the observation model nonlinear equation, yielding the transformed sigma points from the state vector and the covariance, shown earlier.

In the update (correction) step of measurement, the Kalman gain, $\mathcal{K}_{k+1}$, is calculated based on the correlation matrix between the measurement and the observation, $\mathbf{P}_{k+1}^{xy}$, and the innovation matrix, both predicted.

$$\mathcal{K}_{k+1} = \mathbf{P}_{k+1}^{xy}\left(\mathbf{P}_{k+1}^{vv} \right)^{-1}, \ \text{with}$$

$$\begin{cases} \mathbf{P}_{k+1}^{vv} = \sum_{i=0}^{2n} W_i^{(\mathrm{c})} \left[y_{i,k+1} - \hat{\mathbf{y}}_{k+1}^- \right]\left[y_{i,k+1} - \hat{\mathbf{y}}_{k+1}^- \right]^{\mathrm{T}} + \mathbf{R}_{k+1} \\ \\ \mathbf{P}_{k+1}^{xy} = \sum_{i=0}^{2n} W_i^{(\mathrm{c})} \left[\boldsymbol{\chi}_{i,k+1} - \hat{\mathbf{x}}_{k+1}^- \right]\left[y_{i,k+1} - \hat{\mathbf{y}}_{k+1}^- \right]^{\mathrm{T}} \end{cases}$$

Finally, the update state and covariance are

$$\hat{\mathbf{x}}_{k+1}^+ = \hat{\mathbf{x}}_{k+1}^- + \mathcal{K}_{k+1}\left(\mathbf{y}_{k+1} - \hat{\mathbf{y}}_{k+1}^- \right)$$

$$\mathbf{P}_{k+1}^+ = \mathbf{P}_{k+1}^- - \mathcal{K}_{k+1} \, \mathbf{P}_{k+1}^{vv} \, \mathcal{K}_{k+1}^{\mathrm{T}}$$

where $\mathbf{y}$ is the actual measurement vector at the instant $k+1$.

The process is repeated for the next instant. The updated mean and covariance from the present instant will be used to deterministically generate the sigma points of the next instant, cyclically.

RESULTS

Here, the tests and the analysis for the extended and the sigma point algorithms developed to compute all the considered perturbations are presented.

Aspects of computational complexity and processing time between both algorithms were already presented elsewhere (Pardal et al., 2009 (a), (b)).

To validate and to analyze the proposed method, real data from the T/P satellite were used. Position and velocity to be estimated were compared with T/P precise orbit ephemeris (POE), from JPL/NASA. The test conditions considered real L1 pseudo-range data, collected by the GPS receiver onboard TOPEX, on November 19, 1993. The tests covered a long (24 hours) period of orbit determination.

The force model included perturbations due to geopotential up to order and degree (30x30), with harmonic coefficients from JGM-2 model, direct solar radiation pressure, and Sun-Moon attraction. The pseudo-

range measurements were corrected to the first order with respect to ionosphere.

The obtained results were evaluated through one parameter: error in position components, which represents the difference between the POE/JPL reference and the estimated position components. Such parameter is given by

$$\Delta \vec{r} \equiv \begin{bmatrix} x - \hat{x} \\ y - \hat{y} \\ z - \hat{z} \end{bmatrix}$$

which are after translated to radial, normal, and along-track (RNT) components of T/P orbit fixed system.

First, only geopotential were considered for the mentioned period of orbit determination. They were considered two models: a lower order and degree 10, and then a higher order and degree 30. After, the direct solar radiation pressure force acting on T/P center of mass was included, together with the higher geopotential model. And, finally, perturbations due to Sun-Moon attraction were added to the model of forces. Therefore increasing levels of modeling complexity were being added to test the filters.

The obtained data were after translated to RNT system, which interpretation is straightforward. In this system, the radial component "R" points to the nadir direction, the normal "N" is perpendicular to orbital plane, and the transversal (along-track) "T" is orthogonal to "R" and "N", and so is also the velocity component. Thus, it is possible to analyze what happens with the orbital RNT components, and with the orbit evolution as well.

Orbit Propagation

Here the effects of introducing each perturbation gradually are analyzed in the orbit propagation step, before the orbit determination through UKF or EKF. Therewith, it is possible to assert if the model was well implemented or not.

The orbit propagation graphics were plotted analyzing, step by step, the inclusion of each perturbation. First, a model of geopotential spherical harmonics up to order and degree 10; second a more complex geopotential model, up to higher order and degree 30; third, to the complex geopotencial model was added the direct solar radiation pressure; and, finally, the full model of forces was implemented, adding the Sun-Moon gravitational attraction to the third model.

Fig. 3 shows the perturbations effects in orbit propagation. It includes geopotential up to order and degree 10 (geo 10); geopotential up to higher order and degree 30 (geo 30); geopotencial model geo 30 added to direct solar radiation pressure (geo 30 + srp); and, finally the full model of forces is implemented, including also Sun-Moon attraction (geo 30 + srp + sm).
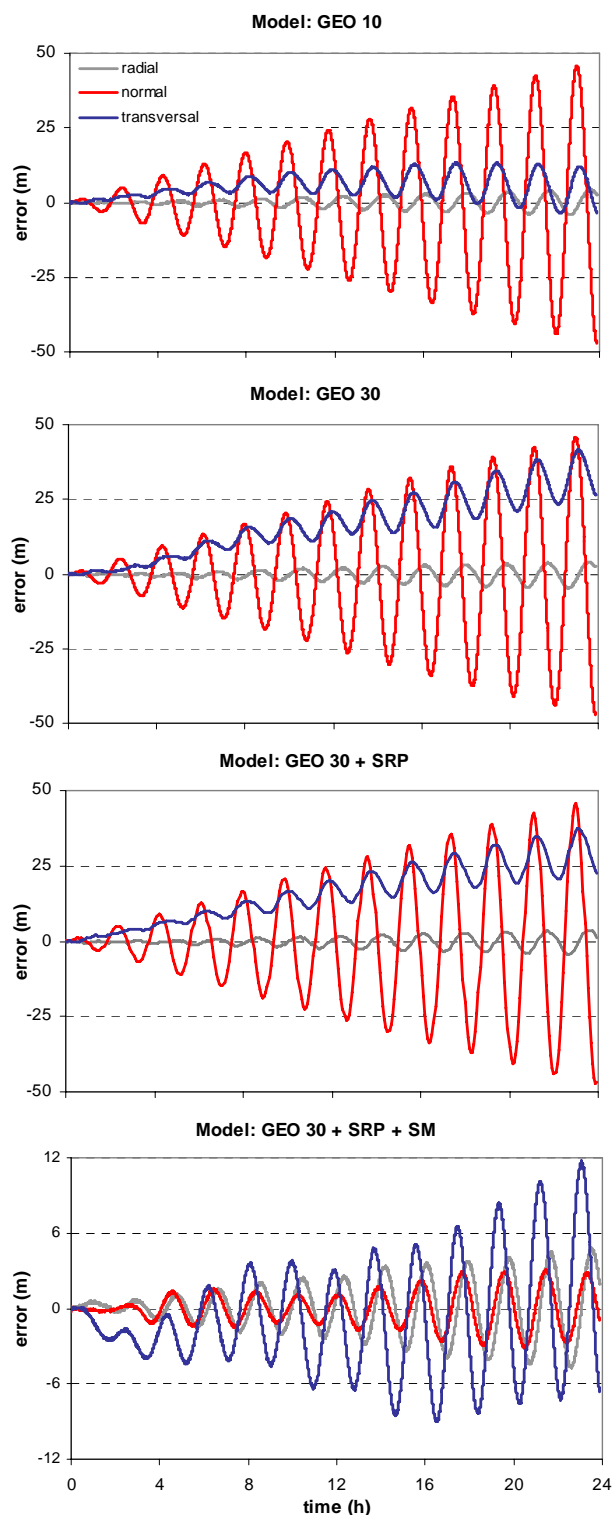

Figure 3. Orbit propagation for models of forces tested, in RNT components, with data from 19 Nov. 1993.

When the geopotential harmonics order and degree was increased from 10 to 30, an anomalous non explained behavior of the transverse component error RMS

2738

23rd International Technical Meeting of the Satellite Division of
The Institute of Navigation, Portland, OR, September 21-24, 2010

increasing occurred. However, the direct solar radiation pressure inclusion did not cause any significant change in the RMS values. And, when the Sun-Moon attraction was included in the dynamical model, the components errors RMS had a meaningful decrease. The RMS values can be checked in Tab.1, as follows. In Tab. 1, "Geo10" means a dynamical model including only perturbations of geopotential spherical harmonics up to order and degree 10; "Geo30", a model including perturbations of geopotential up to higher order and degree 30; "SRP", a model that adds to the "Geo30" the direct solar radiation pressure modeling; and "SM" the complete dynamical model considered, including the last perturbation modeling to the "SRP": the Sun-Moon gravitational attraction.

Table 1. RMS errors values for each model of forces considered in orbit propagation.

Dynamical Model	RMS (m)			
	R	N	T	total
Geo10	1.764	19.812	6.562	20.945
Geo30	1.896	19.891	19.742	28.088
SRP	1.882	19.794	19.703	27.992
SM	2.090	1.367	4.427	5.083

Orbit Determination

In orbit determination, the results were obtained after state estimation by UKF or EKF. As it was expected, due Kalman filters do not completely trust in the dynamical model. Improving the model from a simple geopotential up to a lower order and degree only to a more complex complete model including geopotential, direct solar radiation pressure, and Sun-Moon attraction, did not cause meaningful changes in the RNT components errors values. Also, for a 30s sampling rate, there was not significant differences in the errors values if the estimator used was UKF or EKF.

Fig. 4 presents a typical result obtained, with the errors in RNT components evolution during a long 24 hours period of orbit determination. For this test, sampling rate was 30s. This result was obtained using a model including geopotential up to order and degree 30 and Sun-Moon attraction. Each error component was compared between the UKF estimation results (red curves) and the EKF ones (dark blue curves). Because of the complexity to calculate the direct solar radiation pressure Jacobian matrix, needed to the EKF implementation, and as Sun-Moon attraction is the major effect that shifts the errors values, one decided to compare both algorithms through this most important effect only.
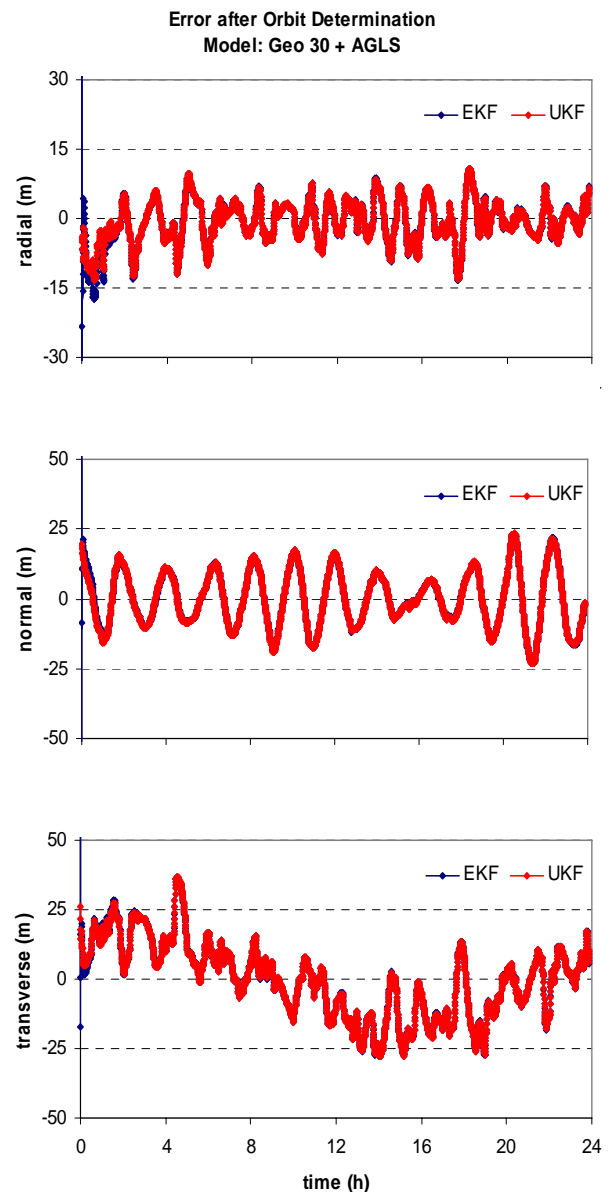

Figure 4. Orbit determination typical result, in RNT components, with data from 19 Nov. 1993.

Tab. 2 presents components and total RMS errors, in meters, for both algorithms. The dynamical models with geopotential up to order and degree 10, geopotential up to order and degree 30, and the model including the Sun-Moon attraction to the geopotential perturbations were estimated by the UKF and EKF. Therefore, the complete model, including the direct solar radiation pressure was implemented only by UKF, for the reasons explained before. Although the statistics are very close, the best results occurred when Sun-Moon attraction was considered in the modeling, as can be seen in Tab. 2. There is also a mean and standard deviation column at left side. As mean and standard deviation are related to RMS through the equation $\text{RMS} \approx \sqrt{(\text{mean})^2 + (\text{std deviation})^2}$,

2739

23rd International Technical Meeting of the Satellite Division of
The Institute of Navigation, Portland, OR, September 21-24, 2010

the results show that statistical consistency was accomplished.

Table 2. RMS errors values for each model of forces considered, and for each estimator used, in orbit determination.

Filter	Dynamical Model	position error (m) mean ± std deviation	RMS error (m)			
			R	N	T	total
UKF	Geo10	17.184 ± 6.569	4.789	11.389	13.634	18.399
	Geo30	16.659 ± 6.491	4.605	10.635	13.617	17.881
	SRP	16.319 ± 6.516	4.576	10.146	13.602	17.575
	SM	16.319 ± 6.519	4.622	10.150	13.629	17.611
EKF	Geo10	17.362 ± 6.964	5.361	11.546	13.711	18.709
	Geo30	16.814 ± 6.903	5.197	10.772	13.690	18.178
	SRP	16.473 ± 6.940	5.170	10.292	13.673	17.227

Predicted Residuals of Pseudorange

As the orbit determination results have shown, the dynamical models accuracy improvement do not improve the errors results between the POE/JPL reference and the estimated position values. Further, such results shows similar competitivity between both estimators.

With the purpose of making a deeper study of the dynamical models accuracy benefits, and of the filters competitiveness, another test was made. Different sampling rates were considered: 10, 30, 60, and 300s. With time scattered measurements, one desired to verify the impact of the different dynamic models, and of each filter in the prediction step (time update). Therefore, predicted pseudorange residuals (innovation) were analyzed.

Fig. 5 was plotted using residuals predicted through UKF, considering a dynamic model with geopotential up to order and degree 30 and Sun-Moon attraction. It shows a typical pseudorange residuals behavior along time, obtained using a 60s sampling rate. This shape behavior manifested similarly for a 10, 30, or 60s rate, independent of the used filter.
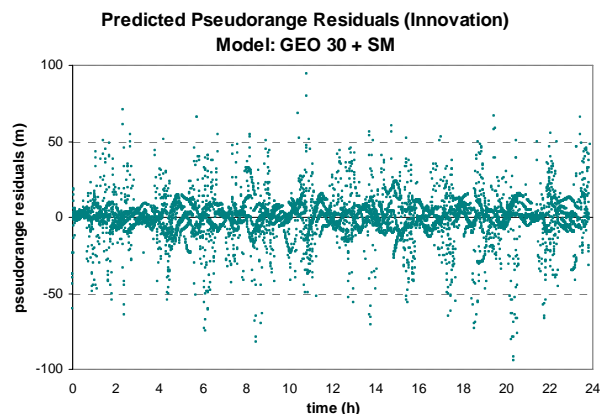

Figure 5. Predicted pseudorange residuals typical behavior obtained by UKF, with a 60s sampling rate, and data from 19 Nov. 1993.

However, through residuals mean and standard deviation values (Tab. 3), it seems that results suggest more scattering when the estimation is made by EKF than by UKF.

The radical test using higher sampling rate of 300s was made in order to verify if the results really implies a higher dispersion (standard deviation) when the estimation is made by EKF than by UKF . Tab. 3 confirmed that the UKF outperforms EKF yielding less dispersed measurement residuals. Thus, pseudorange residuals predicted by UKF are less scattered than the ones by EKF, meaning that the UKF predicted much better the residuals behavior due to its algorithm approach.

As far as the dynamical model is concerned, more accurate models contribute to better results, which means better predicted residuals. Through Tab. 3, if the dynamical model accuracy is increased together with different sampling rates, one can see clearly how the residuals mean behaves as the modeling complexity increases.

Table 3. RMS errors values for each model of forces considered, and for each estimator used, in orbit determination.

Pseudorange Residuals			
Dynamical Model	Filter	sampling (s)	Mean ± Std Deviation (m)
Geo 10	UKF	10	0.124 ± 11.384
		30	0.046 ± 13.685
		60	-0.187 ± 14.690
		300	-22.767 ± 92.790
	EKF	10	0.061 ± 11.372
		30	0.042 ± 13.554
		60	-0.277 ± 16.221
		300	-66.785 ± 142.965
Geo 30	UKF	10	0.122 ± 12.036
		30	0.032 ± 13.465
		60	-0.091 ± 14.363
		300	-1.234 ± 17.489
	EKF	10	0.059 ± 12.027
		30	0.031 ± 13.461
		60	-0.180 ± 15.942
		300	1.861 ± 45.886
SM	UKF	10	0.115 ± 12.547
		30	-0.038 ± 14.178
		60	-0.109 ± 14.021
		300	-1.294 ± 15.872
	EKF	10	0.052 ± 12.539
		30	-0.039 ± 14.055
		60	-0.201 ± 15.639
		300	1.021 ± 43.197
SRP	UKF	10	0.115 ± 12.570
		30	-0.051 ± 13.971
		60	-0.109 ± 14.017
		300	-1.288 ± 15.874

In order to conclude results section, Fig. 6 will show two results of pseudorange residuals plotted for a 300s sampling rate, which values are in Tab.3. It is clear that measurements rejection (at the level of 150m) are higher in EKF estimation than in UKF. Although measurements rejection of outliers occurs in both algorithms, the major

difference is that UKF is able to better adapt to these adverse conditions than EKF and to predict pseudorange more accurately. In Fig. 6 residuals obtained via both UKF and EKF algorithms for the dynamic model including geopotential up to order and degree 30 and Sun-Moon attraction were plotted.
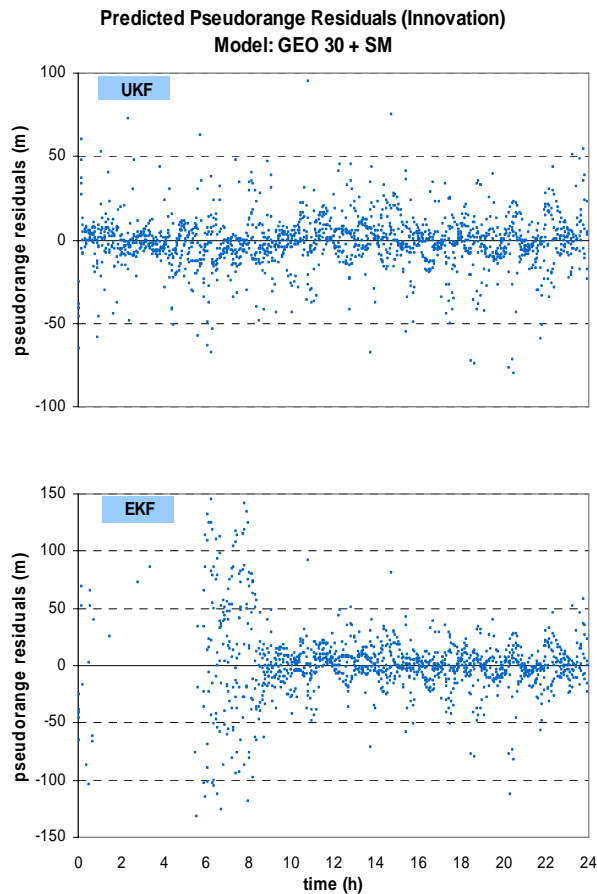

Figure 6. Predicted pseudorange residuals behavior obtained by UKF and EKF, with a 300s sampling rate, and data from 19 Nov. 1993.

CONCLUSIONS

The effects of introducing different levels of perturbations gradually were analyzed in the orbit prediction step (time update), before the measurement update cycle through UKF or EKF. There, it was possible to confirm that the models were implemented accordingly. The direct solar radiation pressure inclusion did not cause any significant change in the position components error. Also, it is noticed that Sun-Moon attraction inclusion is needed to decrease the orbit prediction error.

In the orbit determination using GPS, Kalman filters do not need to trust completely in the dynamical model due to the available redundancy of measurements. The results have shown that dynamical models improvement do not decrease significantly the final accuracy. Also there was not significant differences in the errors whether the estimator used was UKF or EKF, which does not lead us to any conclusive choice between both algorithms.

The analysis of predicted pseudorange residuals for different sampling rates confirmed that for larger sampling rates UKF can predict better the residuals than EKF, with less scattered results. This hints that UKF is probably more robust if other uncertainties are present. Future works should include large initial uncertainties and inaccurate initial covariances to test the aspects of robustness and convergence of both filters.

ACKNOWLEDGEMENTS

REFERENCES

Brown, R.G.; Hwang, P.Y.C.: "Introduction to random signals and applied Kalman filtering". 3. ed. New York: John Wiley & Sons, 1985. 502p.

Chiaradia, A.P.M.; Kuga, H.K.; Prado, A.F.B.A.: "Single frequency GPS measurements in real-time artificial satellite orbit determination" Acta Astronautica, v. 53, n. 2, p. 123-133, 2003.

Julier, S.J.; Uhlmann, J.K.; Durrant-Whyte, H.F.: "A new approach for filtering nonlinear systems". In: American Control Conference, June 1995, Seattle, Washington. Proceedings… TA5 - 9:15, p. 1628-1632.

Julier, S.J.; Uhlmann, J.K.: "A new extension of the Kalman filter for nonlinear systems". International Symposium on Aerospace/Defense Sensing, Simulation and Controls. SPIE, 1997.

Julier, S.J.; Uhlmann, J.K.; Durrant-Whyte, H.F.: "A new method for the nonlinear transformation of means and covariances in filters and estimators". In: IEEE Transactions on Automatic Control, 2000. Proceedings… 2000. v. 45, Issue 3, p. 477-482.

Julier, S.J.; Uhlmann, J.K.: "Unscented filtering and nonlinear estimation". In: IEEE Transactions on Automatic Control, v. 92, n. 3, 2004. Proceedings… Mar 2004.

Jwo, D-J; Lai, C-N.: "Unscented Kalman filter with nonlinear dynamic process modeling for GPS navigation". GPS Solutions. Springer: Berlin, Sep. 2008, vol. 12, n. 4. ISSN 1521-1886 (on-line).

Kaula, W.M.: "Theory of Satellite Geodesy". Blasdell Pub. Co. Walthmam, Mass, 1966.

Lee, D-J.; Alfriend, K.T.: "Precise real-time orbit estimation using the unscented Kalman filter". Advances in the Astronautical Sciences. v. 114, Suppl.: Spaceflight Mechanics 2003, pp. 20, 2003.

Lee, D-J.; Alfriend, K.T.: "Sigma point filtering for sequential orbit estimation and prediction". Journal of Spacecraft and Rockets. v. 44, n. 2, Mar-Apr 2007.

2741

Marshall, J.A.; Antresian, P.G.; Rosborough, G.W.; Putney, B.H.: "Modeling Radiation Forces Acting on Satellites for Precision Orbit Determination". Advances in Astronautical Sciences, AAS 91-357, Vol. 76, Part I, p. 72-96, 1991. Colorado: August.

Marshall, J.A.; Luthcke, S.B.: "Modeling Radiation Forces on Topex/Poseidon for Precision Orbit Determination". Journal of Spacecraft and Rockets, Vol. 31, n. 1, Jan. - Feb, 1994.

Pardal, P.C.P.M.; Kuga, H.K.; Vilhena de Moraes, R.: "Non Linear Sigma Point Kalman Filter Applied to Orbit Determination Using GPS Measurements". Proceedings of the 22nd International Meeting of the Satellite Division of The Institute of Navigation (ION GNSS 2009). p. 1478-1485.

Pardal, P.C.P.M.; Kuga, H.K.; Vilhena de Moraes, R.: "Comparison of Extended Kalman Filter and Non Linear Sigma Point Filter for Orbit Orbit Determination Using GPS Measurements". Proceedings of the 20th International Congress of Mechanical Engineering (COBEM 2009).

Prado, A.F.B.A.; Kuga, H.K. (Eds): "Fundamentos de Tecnologia Espacial". São José dos Campos: INPE, 2001. 220 p. ISBN: 85-17-00004-8.

van der Merwe, R., Wan, E. A., Julier, S.J.: "Sigma-point Kalman filters for nonlinear estimation and sensor-fusion - applications to integrated navigation". In: AIAA Guidance, Navigation, and Control Conference and Exhibit, 16-19 Aug. 2004, Rhode Island. Proceedings… Providence: American Institute of Aeronautics and Astronautics, 2004.

2742

23rd International Technical Meeting of the Satellite Division of
The Institute of Navigation, Portland, OR, September 21-24, 2010